

# Spectrophotometric variability of quasars caused by lensing of diffuse massive substructure: consequences on flux anomaly and precise astrometric measurements

L. Č. Popović<sup>1,2,3★</sup> and S. Simić<sup>2,4</sup>

<sup>1</sup>*Astronomical Observatory, Volgina 7, 11160 Belgrade, Serbia*

<sup>2</sup>*Isaac Newton Institute of Chile, Yugoslavia Branch, Volgina 7, 11060 Belgrade, Serbia*

<sup>3</sup>*Faculty of Mathematics, University of Belgrade, Studentski Trg 16, 11000 Belgrade, Serbia*

<sup>4</sup>*Faculty of Science, University of Kragujevac, Radoja Domanovića 12, 34000 Kragujevac, Serbia*

Accepted 2013 March 18. Received 2013 March 16; in original form 2013 February 11

## ABSTRACT

We investigate the spectrophotometric variability of quasars due to lensing of small mass substructure (from several tens to several hundreds solar masses). The aim of this paper is to explore the milli/microlensing influence on the flux anomaly observed between images of a lensed quasar in different spectral bands and the possible influence of small mass structure lensing of non-macrolensed quasars. We find that spectrophotometric variability may also be caused by lensing of small mass diffuse structure and can produce the flux anomaly, which is sometimes seen in different images of a lensed quasar. Additionally, we found that the lensing by small mass diffuse structure may produce significant changes in the photocentre position of a quasar, and sometimes can split or deviate images of one source that can be detected as separate from the scale from 0.1 to several milliarcseconds. This can be measured with *Gaia*-like space astrometric missions. We point out a special case where a low redshifted deflector ( $z_d \sim 0.01$ ) is lensing a high redshifted source for which the variability in the flux and photocentre (several milliarcseconds) may be detected on a relatively short time-scale.

**Key words:** gravitational lensing: micro – galaxies: active.

## 1 INTRODUCTION

The light from a distant quasar [quasi-stellar object (QSO)], along its path towards the Earth, can be perturbed by compact objects, as e.g. galaxies, stars in galaxies, stellar clusters, intermediate mass compact objects (with  $10^{2-4} M_\odot$ ) and cold dark matter (CDM) structure. This can cause magnification in the luminosity of a QSO and in its photometric position, the so-called lensing effects. The gravitational lensing can be strong or weak, depending on the position of a quasar and object (in the line of sight of an observer) which acts as a lens, if the line of sight from the observer to the source lie very close to the centre of a massive object (galaxy cluster, galaxy, CDM, stellar cusp, etc.) then we expect a strong lensing effect. The strong lensing of QSOs can cause a significant wavelength dependent amplification and affect the photocentric position spectrum (see e.g. Congdon & Keeton 2005; Oguri 2005; Treu 2010; Erickcek & Law 2011). Depending on the image angular separation, the strong lensing can be divided into several categories from

which three are the most used (see Treu 2010; Zackrisson & Riehm 2010): macrolensing ( $>0.1$  arcsec), millilensing ( $10^{-3}$  arcsec) and microlensing ( $10^{-6}$  arcsec). Usually, millilensing and microlensing are considered to be present in the images of a macrolensed QSO; however, the effect of micro/millilensing may be present in QSOs even if they are not macrolensed, i.e. the line of sight from the observer to source does not lie very close to the centre of a massive galaxy, but still a compact massive object from the galaxy and stars can affect the QSO light (see e.g. Zakharov, Popović & Jovanović 2004; Zackrisson & Riehm 2007). There are a number of QSOs observed through a galaxy stellar disc (see e.g. Meusinger et al. 2010). The possibility that QSOs are micro/millilensed seems to be higher than macrolensed. As e.g. Zaharov et al. (2004) found that the optical depth for gravitational micro/millilensing caused by cosmologically distributed deflectors could be significant and could reach from 0.01 to 0.1 for QSOs with  $z > 2$ . Therefore, micro/millilensing effect may be often present not only in the case of lensed QSOs, but also in a number of non-lensed objects. It is well known that micro/millilensing can be used for investigation of the structure of QSOs as well as lensing objects (see e.g. Schmidt & Wambsganss 2010; Treu 2010; Zackrisson & Riehm 2010, for

\*E-mail: ssmic@kg.ac.rs

review), and especially they present a tool for detection of dark matter subhalos (see, e.g. Inoue & Chiba 2005; Chen et al. 2007; Zackrisson & Riehm 2007, 2010; Erickcek & Law 2011, etc.).

Mainly two effects of micro/millilensing are used to investigate structure of quasars and lensed objects: (i) a magnification that may be wavelength dependent due to complex structure of QSOs (see e.g. Popović & Chartas 2005; Jovanović et al. 2008; Sluse et al. 2012; Stalevski et al. 2012), and in a such way producing a continuum (line) flux anomaly in the images of a macrolensed QSO (see e.g. Blackburne, Pooley & Rappaport 2006; Pooley et al. 2006; Kratzer et al. 2011; Pooley et al. 2012, etc.) and (ii) a slight wobbling of the observed source position caused by microlensing effect, called astrometric microlensing (photocentre variations), that presents a photocentroid displacement of the source image during the microlensing event in the lens plane (see e.g. Hog, Novikov & Polnarev 1995; Miyamoto & Yoshii 1995; Walker 1995; Dominik & Sahu 2000; Lee et al. 2010, etc.). In the above papers, it has been shown that for a single lens and a single source configuration, centroid motion during the microlensing event follows, more or less, an elliptical dependence on the impact parameter of the source and lens.

Astrometric microlensing has been explored by a number of authors covering different regimes. Most of them discussed cases where lenses are stars in the Milky Way or dark matter objects in Galactic halo, acting on background stars either in the Magellanic Clouds or in nearby galaxies, as e.g. M31 (see e.g. Miralda-Escude 1996; Boden, Shao & van Buren 1998; Goldberg & Wozniak 1998; Mao & Witt 1998; Paczynski 1998; Han & Kim 1999; Safizadeh, Dalal & Griest 1999; Dominik & Sahu 2000; Delplancke, Gorski & Richichi 2001; Belokurov & Evans 2002; Dalal & Lane 2003; Lee et al. 2010; Proft, Demleitner & Wambsgans 2011; Yano 2012, etc.). The effects of Milky Way stars on background quasars were studied in several papers (see e.g. Hosokawa, Ohnishi & Fukushima 1997; Sazhin et al. 1998; Honma & Kurayama 2002; Sazhin, Sazhina & Pshirkov 2011) as well as the effect of local dark matter subhalos (see e.g. Erickcek & Law 2011). There are also studies that investigate astronomical lensing in intervening galaxy (see Williams & Saha 1995; Chen et al. 2007). However, changing in magnification at different wavelengths (flux anomaly due to micro/millilensing) in combination with astrometric microlensing is rarely investigated.

A new class of satellites will be able to conduct precise measurements of an object photocentre in different spectral ranges. For instance, the satellite *Gaia* is equipped with most sophisticated instruments with astonishing capabilities, producing the accuracy better than 20  $\mu$ s in wide energy range 330–1050 nm. The primary objective of this mission is to not only create a three-dimensional model of our Galaxy, but also to be used in other branches of astronomy, such as detection of extrasolar planets, brown dwarfs, asteroids, exploding stars, testing the Einstein theory, etc. One of the main tasks of this mission is the definition of fixed celestial referential frame, the *Gaia* realization of the International Celestial Reference System (ICRS; Mignard et al. 2002). To reach this purpose, a large number of QSOs (5000–10 000) uniformly distributed over the sky are required. QSOs are active galactic nuclei (AGNs) located at cosmological distances. This makes them a perfect candidate for this purpose as they are objects without or with negligible proper motion. The QSO sample dedicated to this task should exhibit absolutely no proper motion and be completely free from any contaminant (non-QSO objects), while tiny apparent astrometric motions due to inner structure flux variations (Popović et al. 2012) or (micro) lensing are always possible (Treyer & Wambsgans

2004). As we noted above, micro/millilensing may be present also in not macrolensed QSOs. In Popović et al. (2012) we investigated photocentric variability of quasars caused by variations in their inner structure, and here, we give our investigation of the influence of the micro/millilensing of diffuse small mass structure (like an open stellar cluster) on photocentric variation of QSOs that can also have consequence for *Gaia* measurements.

The aim of this paper is to investigate spectroastrometric variability of quasars caused by micro/millilensing taking into account the complex emitting structure of a QSO. Additionally, we consider the lens as a bulk of stars concentrated on a relatively small surface, as e.g. star clusters, simulating a massive diffuse lensing structure that contains between several tens and several hundreds of solar mass stars. We explore astrometric microlensing in combination with spectral variation from the ultraviolet (UV) to infrared (IR) spectra band. This could be of particular interest since both depends on the specific properties of a lens and a source (see Keeton & Moustakas 2009).

The paper is organized as follows. In the next section, we present the source and lens model, in Section 3 we give results of our simulations and discuss results, and finally in Section 4 we outline our conclusions.

## 2 THE SOURCE AND LENS MODEL

To investigate photocentric variation in combination with possible wavelength dependent flux amplification, one has to take into account the complex structure of QSOs, but also consider the lens structure. Here, we assumed that the radiation in the UV and optical band is mainly coming from an accretion disc. On the other side, one cannot expect that a single star in galaxies, which are redshifted more than  $z \geq 0.01$  can produce significant astronomical microlensing; therefore, we considered a massive diffuse structure containing a group of stars distributed in a small surface.

### 2.1 Source model – stratified emission disc in QSOs

An AGN has a complex inner structure, meaning that different parts have emission in different spectral bands, i.e. a wavelength dependent dimensions of different emission regions is present in AGNs (see, e.g. Popović et al. 2012). It is widely accepted that the majority of radiation is coming from the accelerated material spiralling down towards the black hole in a form of an accretion disc. The radiation from the disc is mostly thermalized from outer regions  $R_{\text{out}}$  to the centre, with slight exception at inner radius, i.e. very close to the black hole, where Compton upscattering due to the high mass accretion could have a significant role (see Done et al. 2011).

To take into account the spectral stratification of the source we accepted a model of a standard relativistic, optically thick, geometrically thin, blackbody disc model (see, e.g. Pringle & Rees 1972; Novikov & Thorne 1973; Shakura & Sunyaev 1973) using the effective temperature as a function of the radius (Krolik 1998):

$$T \propto R^{-3/4} (1 - (R_{\text{in}}/R)^{1/2})^{1/4},$$

where  $R_{\text{in}}$  is the inner disc radius. At larger radius this equation could be reduced to  $T \propto R^{-\beta}$ , where in the standard model  $\beta = 3/4$ . Here, we are going to investigate the microlensed radiation from the UV to IR (not in X-ray), therefore, we adopted the thermal emission as the main mechanism.

Taking into account the temperature gradient along the disc we adopted the formalism similar to that in Poindexter, Morgan &

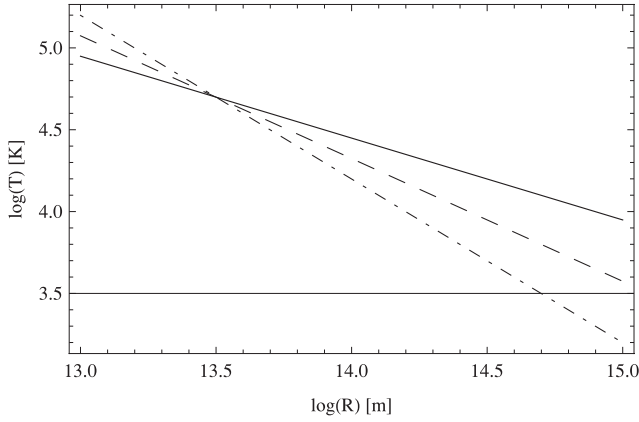


**Figure 1.** Temperature as a function of the position of emitting material in the disc (in logarithmic scale) for different  $\beta$  parameters:  $\beta = 0.5$  – full line,  $\beta = 0.75$  – dashed line and  $\beta = 1.0$  – dash-dotted line.

Kochanek (2008), where the luminosity of a small surface element at the arbitrary position in the disc is proportional to the surface energy density and magnitude of emitting surface (Poindexter et al. 2008)

$$dL(\lambda, R) \propto \frac{dS}{\lambda^5} \left( \exp \left( \frac{hc}{\lambda k \alpha(\beta) R^{-\beta}} - 1 \right) \right)^{-1}, \quad (1)$$

where  $dS$  is the surface element of the source. We replace  $T$  in the expression for the energy density with the distance  $R$  as shown in Fig. 1 and compute the proportionality coefficient as

$$\alpha = T_0 R_0^\beta, \quad (2)$$

where  $T_0$  is the temperature at the distance  $R_0$ . To compute the spectral energy distribution (SED) for the disc configuration we integrate over the whole disc area

$$L(\lambda) \propto \int_{S_{\text{disc}}} dL(\lambda, R). \quad (3)$$

Using equation (3) we calculated the SED of the source (see Fig. 2). As it can be seen in Fig. 2 (up), the SED depends on value of the parameter  $\beta$ , and for  $\beta = 0.5$  (full line) the SED has a maximum at lower energy than other two SEDs (with  $\beta = 0.75$  and  $1$ , dashed and dash-dotted line, respectively). An increase of the source emission is notable at higher energies for higher values of the parameter  $\beta$ .

The inclination of the disc with respect to the observer could be incorporated with additional  $\cos(i)$  ( $i$  inclination angle). In all cases we considered a face-on disc ( $i = 0$ ).

Using the disc model for the continuum emission of QSOs we were able to model emission in the spectral range that will be covered by *Gaia* (see Fig. 2, down). Moreover, such model allowed us to explore, both flux anomaly and photocentre variation in different spectral bands during a micro/millilensing event.

## 2.2 Lens model–diffuse massive substructure

As we noted above, the light from distant QSOs may cross far enough from a galaxy that is not macrolensed, but still may be micro/millilensed by structures which belong to the galaxy. Single star, or randomly distributed stars in the galaxy will probably act as a weak lensing, that is out of the scope of this paper.

However, the light may cross near the centre of some massive structures which have significant surface density that can produce

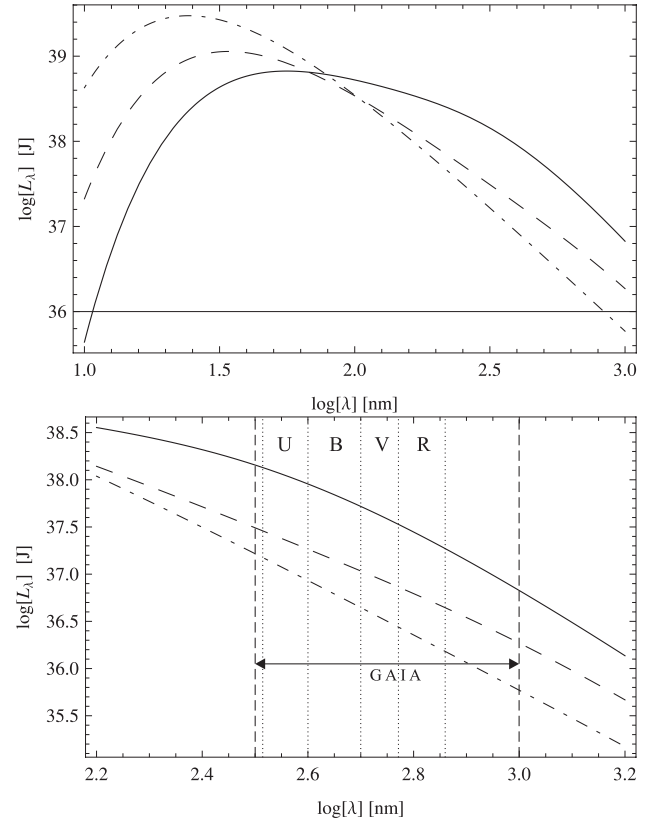


**Figure 2.** The SED of a modelled source for three values of  $\beta$  (notation is the same as in Fig. 1). Upper: for a wide spectral range. Bottom: for  $U, B, V, R$  filters (separated by dotted verticals), which are considered in the paper and also the spectral range which will be covered by *Gaia* is also shown.

strong (micro/milli) lensing effect. As widely accepted, galaxies can contain substructures with few tens to few hundreds stars which are usually addressed as the open star clusters. They can be irregular in shape with dimension of a few parsecs or less. Here, we will discuss effects of group of stars usually referred as an open star cluster that contains from a few tens to few hundreds Sun-like stars.

Such substructures contain enough stars to be able to produce the gravitational lensing on milli/micro scale. Here, we investigate such structure as a possible lens. For magnification map simulation, we used the ray-shooting technique, and first we describe the technique in a few sentences.

### 2.2.1 Generation of micro/millilensing magnification maps

A distribution of stars in the lens plane generates microlensing magnification map in source plane which could be computed by the ray-shooting technique (Kayser, Refsdal & Stabell 1986; Schneider & Weiss 1986, 1987; Treyer & Wambsganss 2004). This technique proposes to follow a ray of light from the observer point passing towards the lens and falling on the source plane. Light rays initiated with different angles close to the observer will have different deflection angles at the lens plane and reach the source plane at different points. We place the grid in the source plane and count the number of light rays falling on to particular grid cells. In that way, the unique map is created representing the current star distribution in the lens plane. This map is called the magnification map and can be used to determine the amount of magnification of source imposed by the lens. In Fig. 3, we present a sketch of the ray-shooting technique.

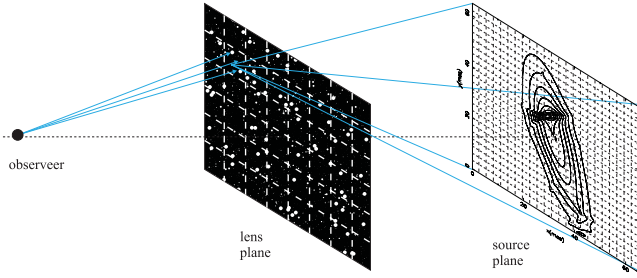


**Figure 3.** A schematic representation of the ray-shooting technique in which a beam of light rays is shot from the observer through the lens plane towards the source. In the source plane, we sketch the source with concentric curved lines.

### 2.2.2 Distribution of deflectors in the lens plane

A microlens is often defined as a random distribution of sun-like stars with masses equal to  $M_{\odot}$ , over the lens surface. This distribution is determined by the parameter  $\kappa$ , which presents average surface density. In nature, stars are mostly distributed in clusters with different shapes. Therefore, considering the discussion at the beginning of Section 2.2 here we used a random star distribution with the application of a scale parameter  $\chi$ , which could allow us to change the compactness of the star cluster. Also, we can simulate density perturbation in a form of star groups in order to produce galaxy substructures mentioned in Section 1. Additionally, we have adopted a thin lens approximation, which assumes that all stars belonging to the lens are placed in one plane. This approximation is acceptable when the lens and source are at cosmological distances, so we neglect the dimensions of the lens itself.

First, we randomly distributed a number of solar mass stars  $N_{\text{lens}}$  in the circular area with angular diameter  $d_l$ . In the source plane of a squared shape with dimension  $d_s$ , we considered a grid of  $N \times N$  pixels, where one pixel has dimension of  $d_s/N$ . The deflection angle has been calculated using the gravitational potential in each point of the lens plane as

$$\alpha = \nabla\psi \quad (4)$$

For the calculation of the gravitational potential we solved the Poisson equation  $\nabla^2\psi = 2\kappa$  in the lens plane, and we used the lens equation for computing the coordinates of points (elements of the source plane grid) where light ray will fall. This process has been repeated a number of times for different incoming angles in order to produce the light rays distribution on the source plane, i.e. to generate the magnification map. The magnification of a point on the map is higher if more light rays fall on it. Those light rays are then distributed over all pixels in the source plane, and the number of rays per pixel is proportional to the magnification due to microlensing at that pixel in the source plane.

Using a magnification map created in described way in the source plane, we considered a source of light of a finite dimension  $d_{\text{src}}$ , that is also divided in a number of pixels. We accounted only for the light rays falling on the source itself or better to say rays emitted from the source surface. That radiation is additionally increased by the amount defined with distribution of caustics of magnification map in particular pixels. The emission of source pixel is determined by its SED. Depending on the lens mass distribution, in the scope of the ray-shooting technique, there can be more than one pixel in the lens plane where light rays sent from the observer penetrate and fall on the particular pixel in the source plane. Finally, any pixel

of source has a collection of pixels in the lens plane that depends on its SED. This procedure allowed us to create an image of the source in the lens plane in considered spectral range. Luminosity of the lens plane pixel  $L_{\text{pix}}^{\text{lens}}(\lambda)$  is higher if there are more light rays passing through it and mathematically presents a sum of SEDs for all passed light rays:

$$L_{\text{pix}}^{\text{lens}}(\lambda) = \sum_{\text{nrays}} L(\lambda, R). \quad (5)$$

We calculated the centroid shift of the image for a spectral filter as

$$D_{\text{cs}}(F) = \frac{\int_F \sum_{\text{npix}} x_{\text{pix}} L_{\text{pix}}^{\text{lens}}(\lambda) d\lambda}{\int_A \sum_{\text{npix}} L_{\text{pix}}^{\text{lens}}(\lambda) d\lambda}, \quad (6)$$

where  $F$  denotes integration for a particular  $(U, B, V, R)$  spectral band and  $A$  is the whole energy range.

The magnification for a particular source image is computed as the ratio of the luminosity for all pixels in a spectral range with the luminosity in the same spectral range without lens influence, as

$$m(F) = \frac{\int_F \sum_{\text{npix}} L_{\text{pix}}^{\text{lens}}(F) d\lambda}{\int_F \sum_{\text{npix}} L_{\text{pix}}^{\text{no lens}}(F) d\lambda}. \quad (7)$$

The relevant length-scales for microlensing is the dimension of the Einstein Ring Radius (ERR) in the lens plane, defined as

$$\xi_0 = \sqrt{\frac{4Gm}{c^2} \frac{D_d D_s}{D_s}}, \quad (8)$$

and its projection in the source plane is

$$\text{ERR} = \frac{D_s}{D_d} \xi_0 = \sqrt{\frac{4Gm}{c^2} \frac{D_s D_{ds}}{D_d}}, \quad (9)$$

where  $G$  is the gravitational constant,  $c$  is the speed of light,  $m$  is the microlens mass. We adopted standard notation for cosmological distances to the lens  $D_d$ , source  $D_s$  and between them  $D_{ds}$ .

Time-scales for microlensing event is described in detail in the book on gravitational microlensing (see Schneider, Ehlers & Falco 1992; Zakharov 1997; Petters, Levine & Wambsganss 2001). Based on the sizes of the source ( $R_{\text{src}}$ ) and caustic ( $r_{\text{caustic}}$ ) pattern we distinguish two cases, when  $R_{\text{src}} > r_{\text{caustic}}$  and  $R_{\text{src}} < r_{\text{caustic}}$  (presented in detail in Jovanović et al. 2008). Both cases could be expressed in a single form

$$t_{\text{crossing}} = (1 + z_d) \frac{R}{v_{\perp} (D_s/D_d)}, \quad (10)$$

where  $R$  replaces the  $R_{\text{src}}$  or  $r_{\text{caustic}}$ . Here, we used a simple approach, since we considered that a microlensing event duration corresponds to the time needed for crossing over the caustic network created by the lens. In this way, the dimension of the caustic patterns in the magnification map determine the total time-scale for particular event, and it can be computed by using the equation (10), with the  $R$  replaced by the dimension of map  $r_m$ . We used already introduced comoving distances  $D_s$  and given map dimensions in ERRs to calculate maps linear dimensions, and hence width of the caustic network.

In all calculations we assumed a flat cosmological model, with  $\Omega_M = 0.27$ ,  $\Omega_{\Lambda} = 0.73$  and  $H_0 = 71 \text{ km s}^{-1} \text{ Mpc}^{-1}$ .

### 2.3 Parameters of source and lens

Source is defined with the inner and outer radius. As we adopted the standard model for the disc we considered that the most of the

radiation in the observed energy range, is coming from the disc part defined with the  $R_{\text{in}} = 10^{13}$  m and  $R_{\text{out}} = 10^{15}$  m, see Blackburne et al. (2011). For evaluating the proportionality coefficient  $\alpha$ , given by equation (2), we took the temperature of  $T_0 = 2 \times 10^4$  K, with the peak radiation around 150 nm, at the radius  $R_0 = 3.15 \times 10^{13}$  m. The coefficient  $\beta$  usually has the value of  $\beta = 3/4$  and we kept that value constant throughout all simulations. The disc inclination can be changed, but in the most simulations we assumed a face-on disc orientation. The source plane dimension is the same in all our computation and equal to 40ERR.

The lens has been assumed to have a circular shape, containing  $N_s$  stars of solar mass ranging from 40 to 240. We also assumed that lens and source are placed at the cosmological distances, with  $z_d = 0.5$  and  $z_s = 2.0$  (standard lens). Those values are not constant in the case when we examine dependence on the source lens distance. We are confident, based on the discussion in Section 2.2 that such carefully chosen lens reflects good enough condition for the gravitational bound systems. Any more massive and densely populated lens will act as one compact object with known influence on the distant source.

### 3 RESULTS AND DISCUSSION

As illustrations, we presented in Fig. 4 the lens with random distribution of 40 and 240 stars (the distributions of stars located at  $z_d = 0.5$  are shown on upper panels, and proper magnification maps for a source at  $z_s = 2.0$  on bottom panels). As it can be seen from Fig. 4, an increase of the star density shows that the lens is very similar to the point-like one, therefore, we considered the maximal star number as 240 solar masses stars. The source images in  $U$ ,  $B$ ,  $V$  and  $R$  filters are shown in Fig. 5. As it can be seen the source images are different in dimension for different filters, and

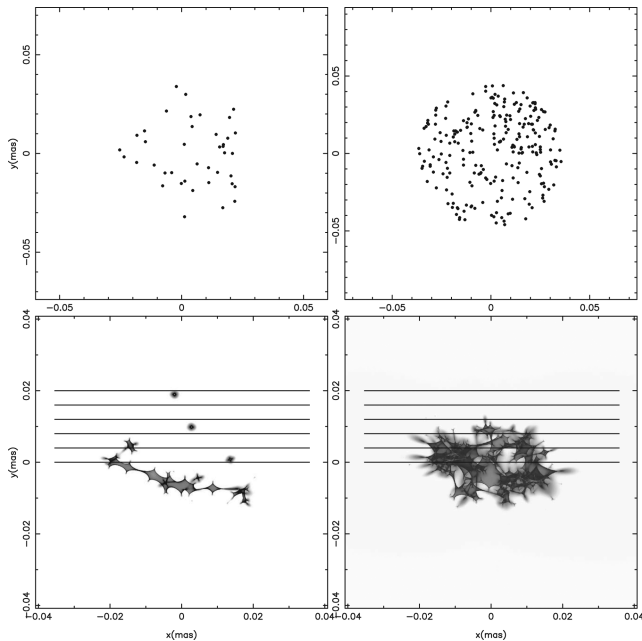


**Figure 4.** Upper panels show a randomly star distribution in the lens plane: (a) case of  $n_{\text{lens}} = 40$  (left-hand panels) and (b) case of  $n_{\text{lens}} = 240$  (right-hand panels). In the bottom panels, we give the appropriate magnification map in the source plane for specified  $n_{\text{lens}}$ , respectively. The horizontal parallel solid lines present the paths of the source for which we calculated magnification light curves and variability of the photocentre positions. These plots are given for a standard lens system with  $z_d = 0.5$  and  $z_s = 2.0$ .

there is an expected magnification in size, that is increasing for the lower energies. Also, there is a notable change in the source structure due to the microlens effect that depends on the lensing system, as well as on the emission region of the source. In the case of  $N_s = 240$ , which we considered as the massive lens, the images are composed from several bright similar structures in all filters, but one can see that the dimensions of bright structures are different. The images of almost point-like source, in this case, are extensive and could be with dimensions of 0.1 mas (see Fig. 5 right). It means that e.g. a non-strongly lensed quasar, due to lensing by diffuse small mass structure, may show a complex shape with different bright spots in the centre and arc-like structures on the edge.

In some cases, one can expect that an image of the source is splitted into several components. Especially, in the case with low redshifted lens and high redshifted source. As an example in Fig. 6 we presented the images in different filters in the case where source is located at  $z_s = 2.0$  and lens at  $z_d = 0.01$ . It is interesting that the lensed source can be seen as several images distributed across several milliarcseconds. This can affect a relatively strong jitter in the photocentre of a source, since random distribution of caustics contribute to the source amplification.

In the next section, we present the influence of different parameters to the magnification and photocentre offset in the case where the lens is a stellar system with mass from 40 to 240 solar masses.

#### 3.1 Population of the stars in the lens

It is well known that a single lens microlensing of a source can cause a centroid motion, or wobbling of the photocentre of the source (see e.g. Hog et al. 1995; Miyamoto & Yoshii 1995; Walker 1995; Dominik & Sahu 2000; Lee et al. 2010, etc.). Here, we considered an open cluster configuration of the lens, taking different number of stars, ranging from 40 to 240 solar mass stars, on the same surface. We performed the simulations for a typical gravitational lens system, taking  $z_d = 0.5$  and  $z_s = 2.0$ . The results of our simulations are presented in Fig. 7 and in Table 1. Fig. 7 (upper panels) presents the variation of magnification for six different star numbers in the lens, ranging from 40 to 240. They are grouped and randomly distributed in a circular shape with diameter around 0.08 mas, as it is shown in Fig. 4. As it can be seen from Fig. 7 (upper panels), a significant difference between magnification in different filters is present for massive lens ( $N_s \geq 100$ ), and can be very prominent, i.e. the magnification in the  $U$  filter is significantly higher than in the  $R$  one, and as it can be seen in Table 1, the magnification can be around 1.4 times higher in the  $U$  filter than in the  $R$  one. This can also affect the flux anomaly between different images of a lensed quasar. On the other side, the light curves in different filters have similar shapes, and it is expected that with a higher lens mass (higher stellar density) the lens acts as a point-like lens, i.e. the light curves have a Gaussian-like shape (see Fig. 7, upper – panel right-down). In the case of low-density star clusters we can distinguish separate peaks in the magnification curve induced by the absence of caustics over the source path.

The photocentre variability for considered cases is given in Fig. 7 (bottom panels) and maximal photocentre offset in Table 1. As it is expected, the photocentre variability is higher for massive lens. Fig. 7 (bottom panels) also shows that in almost all cases a decrease of the photocentre offset with approaching the centre of the diffuse mass lens is seen, and the drop is higher for the massive lens. As it can be seen in Fig. 7 (bottom

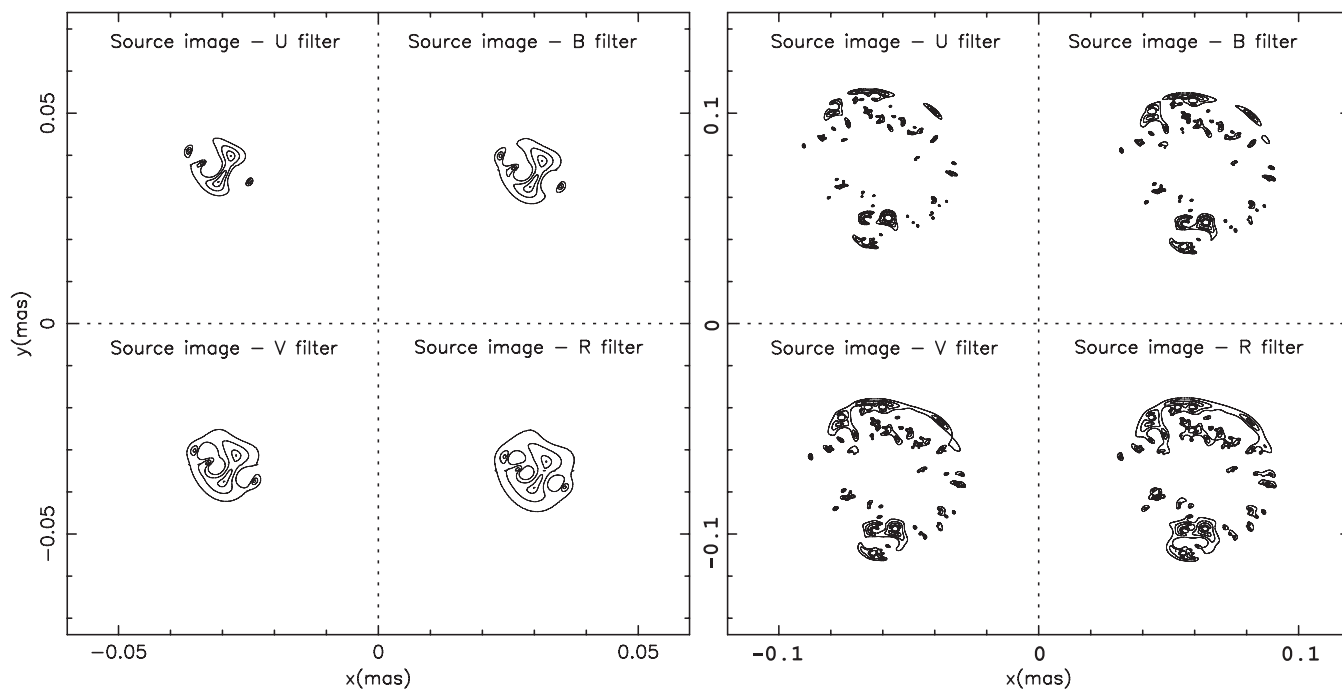


**Figure 5.** Images of source in four different energy channels  $U$ [332–398 nm],  $B$ [398–492 nm],  $V$ [507–595 nm] and  $R$ [589–727 nm]. Lens for this case is presented in Fig. 4. Left four panels present the image for the case of  $m_{\text{lens}} = 40$ , while four on the right-hand side are for the  $m_{\text{lens}} = 240$  stars, with mentioned  $z_d = 0.5$  and  $z_s = 2.0$ .

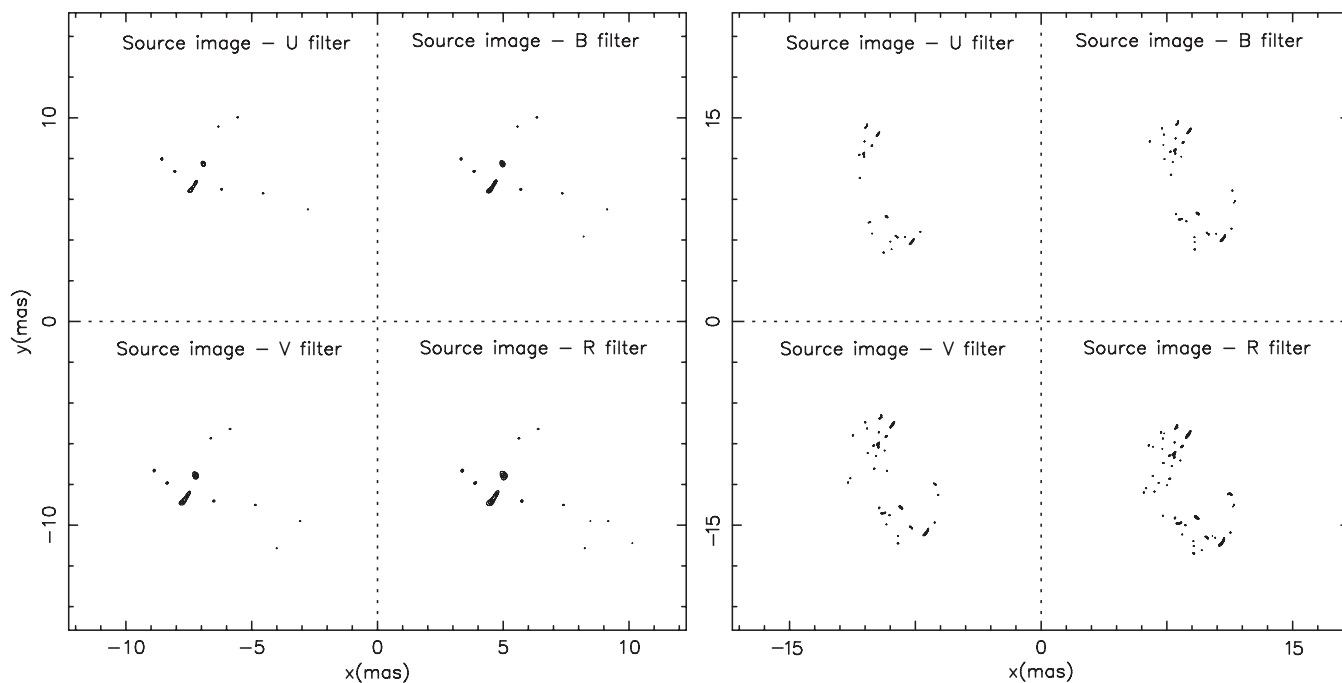


**Figure 6.** The same as in Fig. 5, but for  $z_d = 0.01$  and  $z_s = 2.0$ .

panels) and Table 1 in difference with the magnification, there is no significant photocentre offset difference among different filters with exception for the last two cases of 200 and 240 stars. We conclude that for cluster with higher star population this mutual band deviation will not increase significantly, regarding the single lens behaviour of the lens. The maximal photocentre offset is small, around 0.06 mas for the case of a high density cluster (see Table 1).

### 3.1.1 Different lens and source redshifts

It is interesting to explore a situation where star clusters, containing between several tens and 240 stars, are located at low redshift and act as lenses to different redshifted quasars. Therefore, we performed numerical simulations, assuming that the lens is a low redshifted star cluster ( $z_d = 0.01$ ). The linear dimension of the lens is held constant, consequently when moved closer to the observer its angle

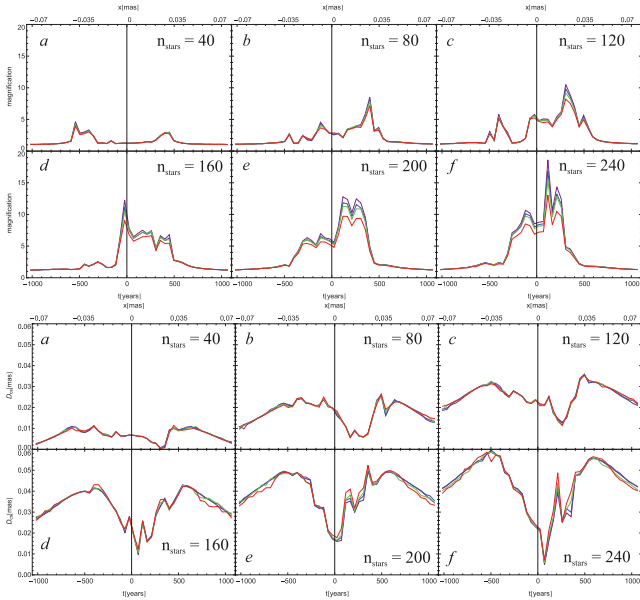


**Figure 7.** Magnification (upper) and centroid shift (bottom) variation for different star numbers in the lens. Different line colours represent observed energy channels,  $U$ [332–398 nm] – violet line,  $B$ [398–492 nm] – blue line,  $V$ [507–595 nm] – green line and  $R$ [589–727 nm] – red line.

**Table 1.** Data for the maximal centroid shift in (mas) and magnification per energy channel for different number of stars in the lens, ranging from 40 to 240. First column gives the number of micro lenses  $n_{\text{lens}}$ , next four are centroid shift in  $U$ ,  $B$ ,  $V$  and  $R$  energy channels, and next four are magnification variability in same channels. Calculations are made for the standard lens and source distances.

$n_{\text{lens}}$	$\kappa$	$d_{\text{fc}}(\text{mas})$				Magn.			
		$U$	$B$	$V$	$R$	$U$	$B$	$V$	$R$
–	–	$U$	$B$	$V$	$R$	$U$	$B$	$V$	$R$
40	0.0940	0.011	0.011	0.011	0.011	4.6	4.4	4.2	3.9
80	0.1620	0.026	0.025	0.024	0.026	8.5	8.1	7.8	7.1
120	0.2182	0.035	0.035	0.035	0.035	10.5	9.8	9.1	8.2
160	0.2650	0.042	0.043	0.042	0.043	12.2	11.2	10.4	9.0
200	0.3070	0.050	0.049	0.051	0.052	12.7	11.8	11.2	9.7
240	0.3440	0.058	0.059	0.058	0.058	18.6	16.9	15.4	13.0

diameter is increased. The lens contains 80 solar mass stars concentrated in a circular shape with diameter 2.7 mas. The distance of a source is changed from  $z_s = 0.05$  to 2.0.

Results of simulations are presented in Fig. 8, and maximal photocentre offset and magnification in Table 2. As it can be seen from Fig. 8 and Table 2, the amplification is almost constant after  $z_s = 0.5$  source redshift and photocentre offset also stays almost the same, taking values around 3–5 mas. Therefore, one can note that a low redshifted star cluster acting as a lens will produce similar amplification and photocentre offset on all high redshifted quasars. In all cases, a flux anomaly is presented and as it is expected, due to dimension of the UV emitting region, the highest amplification is seen in the  $U$  filter.

On the other hand, the time-scales of the lens passing the lens across the source are smaller, and consequently a high variability in the flux can be detected in a period of several years (see Fig. 8). This indicates that high redshifted sources projected very close to the centre of a low redshifted galaxy can be affected by gravitational

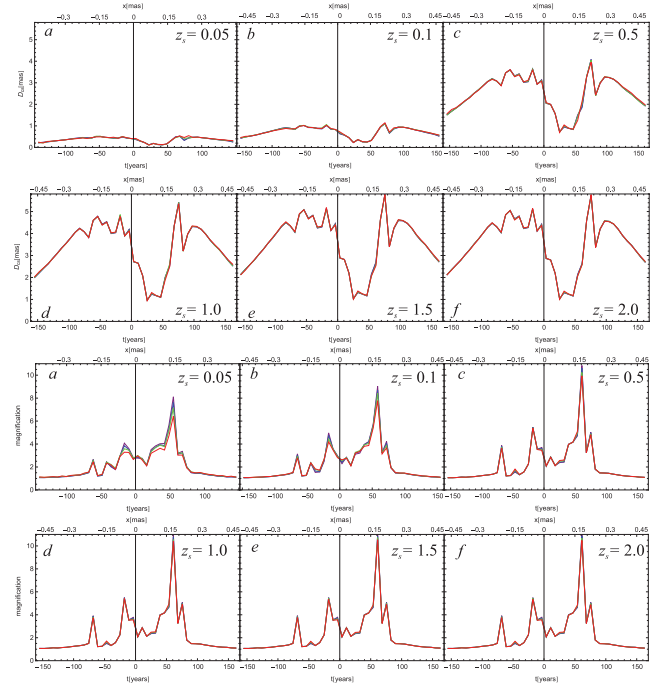


**Figure 8.** Same as in Fig. 7, but for different values of source redshift  $z_s$  and the lens contains 80 solar mass stars.

**Table 2.** Same as in Table 1, but for different values of source distance defined with  $z_s$ , ranging from 0.05 to 2.0. The results are given for the case when the lens contains 80 solar mass stars ( $\kappa = 0.162$ ) located at close distance of  $z_d = 0.01$ .

$z_s$	$d_{\text{fc}}(\text{mas})$				Magn.			
	$U$	$B$	$V$	$R$	$U$	$B$	$V$	$R$
0.05	0.52	0.51	0.52	0.54	8.11	7.61	7.15	6.43
0.1	1.11	1.10	1.10	1.14	9.03	8.69	8.44	7.77
0.5	4.07	4.07	4.04	3.95	10.84	10.61	10.24	9.94
1.0	5.42	5.41	5.40	5.35	10.93	10.78	10.55	10.41
1.5	5.78	5.76	5.75	5.78	10.95	10.84	10.72	10.53
2.0	5.74	5.74	5.74	5.77	10.96	10.87	10.67	10.48

microlensing by small mass clusters, and therefore, they are not suitable candidates for astrometry.

### 3.2 Influence of impact parameter of the microlensing event

All above simulations have been performed for a source crossing the centre of a stellar cluster (lens), but there is possibility that the projected distance between the lens and source is different. Therefore, we simulated cases of different impact parameters  $b$ , for a small mass (40 stars) and more massive (240 stars) lens, taking a standard lens system ( $z_d = 0.5$  and  $z_s = 2.0$ ).

The parameter  $b$  is given in relative units in comparison with the source plane half height and has been changed from 0 (when the lens and source are centred) to 0.5 (lens located at the half height of the lens plane). We simulated transition of the lens taking paths as presented in Fig. 4 (horizontal lines, the line crossing the centre corresponds to  $b = 0$  and the outer one to  $b = 0.5$ ).

For this simulation, we selected two extreme cases with 40 and 240 stars in the lens in order to have a clear picture of what happens during the variation of this parameter. We showed them in the

**Table 3.** Same as in Table 1, but for different values of impact parameters of the source and lens, ranging from 0 to 0.5 of map half height. Paths of source over the magnification map are presented with full lines in Fig. 4. We give the results for two cases when lens contain 40 and 240 stars ( $\kappa = 0.094$  and  $\kappa = 0.344$ , respectively).

$b$	$n_{\text{stars}}$	$d_{fc}(\text{mas})$				Magn.			
		$U$	$B$	$V$	$R$	$U$	$B$	$V$	$R$
0	40	0.010	0.011	0.011	0.011	4.6	4.4	4.2	3.9
0	240	0.058	0.059	0.058	0.058	18.6	16.9	15.4	13.0
0.1	40	0.014	0.014	0.014	0.014	6.4	6.1	5.9	5.4
0.1	240	0.058	0.059	0.058	0.059	21.3	19.1	16.9	14.2
0.2	40	0.018	0.018	0.018	0.019	5.7	5.5	5.5	5.2
0.2	240	0.062	0.061	0.063	0.063	20.3	18.0	15.8	13.2
0.3	40	0.022	0.022	0.022	0.022	1.6	1.5	1.6	1.5
0.3	240	0.062	0.062	0.063	0.065	5.4	5.1	5.0	4.5
0.4	40	0.023	0.023	0.023	0.023	3.2	3.1	3.0	2.9
0.4	240	0.064	0.065	0.064	0.064	2.3	2.3	2.3	2.1
0.5	40	0.024	0.023	0.024	0.023	1.1	1.1	1.1	1.1
0.5	240	0.066	0.067	0.067	0.067	1.3	1.3	1.3	1.3

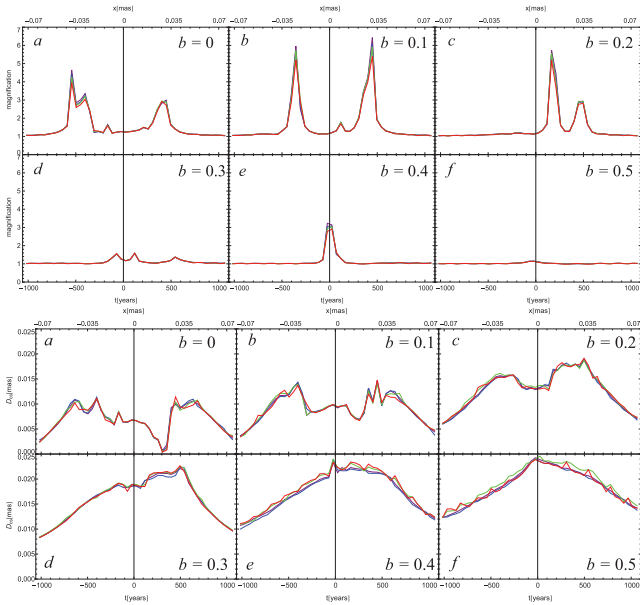


**Figure 9.** Magnification (upper panel) and photocentre (bottom panel) variability of a source during the overcrossing event. Lens consist of 40 solar mass stars distributed uniformly in the circular area with the diameter of 0.04 mas. In panels from (a) to (f) impact parameter  $b$  changes from 0 towards maximum value equal to the half of the half height of source map. Trajectories are presented as in Fig. 4. Distances  $D_d$  and  $D_s$  are defined with its respectful redshifts with values for the standard lens ( $z_d = 0.5$  and  $z_s = 2.0$ ).

form of Table 3 and Figs 9 and 10. For example, in Fig. 9 (upper panel) we see that for the case of lens with 40 stars, there are more or less similar diagrams with casual peaks of the magnification having similar height. Those are caused by a rare caustic distribution in the magnification map for a small number of stars. One can conclude that one peak in light curves presents a variation caused by a single caustic in the map (caused by a group of stars), with relative variation as much as five to seven times. On the contrary, in the second case (Fig. 10), with a more massive lens (240 stars) we have the proportionally higher relative magnification of the order

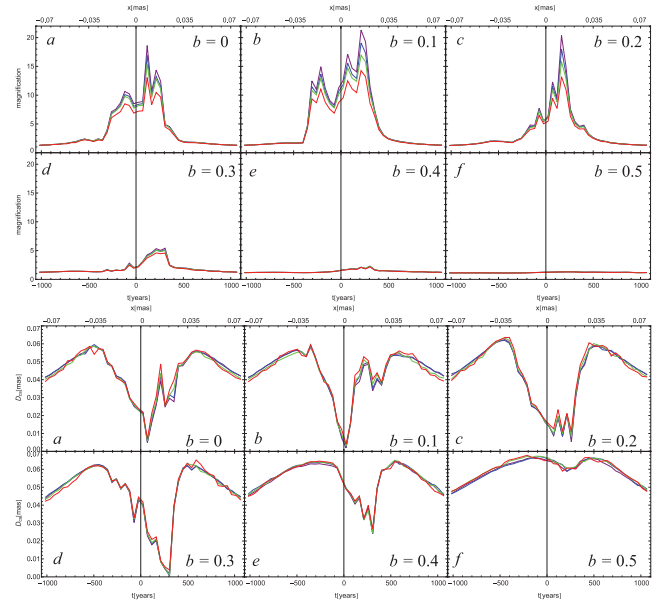


**Figure 10.** Same as in Fig. 9, but for cluster of 240 solar mass stars.

of 20 times, caused by an action of a bulk of overlapping caustics which gradually decreases with an increase of parameter  $b$ . For the last two cases [(e) and (f) in Fig. 10] the magnification is neglected. Such behaviour suggests that the lens acts as a compact object with the mass equal to the sum of masses of all stars in the cluster. In both cases, relative deviations per observed energy channels are at maximum for the moment of the highest magnification with the maximum in the  $U$  channel and decreased for another channels. These observed properties are more clearly given in Table 3, column magn.

For the case of the centroid shift variable  $D_{CS}$  presented in Figs 9 and 10 (bottom panels) for both cases of 40 and 240 stars we can note a lot of similarities with main difference in the amount of shift which is two to three times higher, for latter. For the both cases, we have two peaks which are evolving with increasing of the parameter  $b$ .

The most interesting is that in the case of low-mass cluster, where one can expect almost same magnification and photocentre variation in all passbands form  $b = 0$  to 0.5. Such behaviour is caused since randomly distributed groups of stars can be homogeneously distributed within the cluster.

## 4 CONCLUSIONS

In this paper, we studied the microlensing effect caused by a small mass (diffuse) stellar cluster (up to 240 solar masses) defined in Section 2.2 on the compact QSO source as it is defined in Section 2.1. The case of such lensing may be present in the case of a gravitational lens system, where one of the images can be affected by the lensing of a low-mass cluster. Moreover, this can be present in the case of quasars which are not strongly lensed by the central mass of a galaxy, but they are projected close to the centre of a low redshifted galaxy. In the most cases, we considered a typical lens system ( $z_d = 0.5$  and  $z_s = 2.0$ ) for a low-mass cluster having 40 or 80 solar mass stars in a circular shaped surface with diameter of around 0.08 mas. We explored situations with different distances of a source, taking that the lensing stellar cluster is low redshifted ( $z_d = 0.01$ ). We investigated variations of magnification and photocentre in different ( $U, B, V, R$ ) spectral bands, covering the spectral

range that will be observed with the *Gaia* space mission. From our investigations, we are able to point out the following conclusions.

(i) A small mass stellar cluster (from 40 to 240 solar mass stars) can significantly contribute to the flux and photocentre variability, not only in the case of lensed quasars, but also in the case of quasars which are projected very close to the centre of a low redshifted galaxy. The amplification is different in different spectral filters, ranging from 5 to 20 times; the UV spectrum is more amplified than the IR one. On the other side, the photocentre variability can reach several milliarcseconds, that can be detected with future missions.

(ii) The lensing of such cluster can significantly contribute to the flux anomaly observed in some lensed quasars. In this anomaly, one can expect that the flux in the *U* filter will be always more amplified than in the *R* filter. This shape of amplification can be used to clarify the source of the anomaly. On the other hand, the photocentre offset is not significantly different in different filters. In the case of  $N_L \leq 100$  lensing, one can expect that the image of a lensed quasar or non-lensed quasar has a structure showing brighter spots around the centre and arc-like structures on the edge of the projected Einstein ring of the cluster. Extremely, in the case of low redshifted lens ( $z_d \leq 0.01$ ) and high redshifted source ( $z_s \geq 0.5$ ), there may be several features (or point-like images) separated by several milliarcseconds.

(iii) In a difference with the point-like lens, the diffuse stellar cluster microlensing can produce several prominent peaks in light curve during the lensing event, especially in a low-mass cluster (up to 100 solar mass stars distributed in the considered surface of 0.08 mas). It depends on surface stellar distribution across the projected surface of the cluster, and in the low-mass stellar cluster, the caustics caused by grouping of stars can significantly affect the amplification (different in different spectral filters), as well as cause an offset in the photocentre.

Additionally, we should emphasize a special case with a low redshifted small mass cluster ( $z_d \leq 0.01$ ) in combination with high redshifted quasars ( $z_s \geq 0.5$ ). The effect of lensing in this case is very important, the light of quasars may be amplified in a relatively short period (several years), and photocentre variability can be detected in a relatively short time. Thus, quasars projected very close to the low redshifted galaxies might not be good candidates for the reference frame objects. In this case, one can expect maximal offset of the photocentre of several milliarcseconds, that is comparable with the offset of the photocentre caused by the changes in the inner quasar structure (see Popović et al. 2012).

## ACKNOWLEDGEMENTS

This work is a part of the project (176001) ‘Astrophysical Spectroscopy of Extragalactic Objects’ supported by the Ministry of Science and Technological Development of Serbia. We would like to thank the anonymous referee for very useful comments and suggestions.

## REFERENCES

Belokurov V. A., Evans N. W., 2002, *MNRAS*, 331, 649  
 Blackburne J. A., Pooley D., Rappaport S., 2006, *ApJ*, 640, 569  
 Blackburne J. A., Pooley D., Rappaport S., Schechter P. L., 2011, *ApJ*, 729, 34  
 Boden A. F., Shao M., van Buren D., 1998, *ApJ*, 502, 538  
 Chen J., Rozo E., Dalal N., Taylor J. E., 2007, *ApJ*, 659, 52  
 Congdon A. B., Keeton C. R., 2005, *MNRAS*, 364, 1459  
 Dalal N., Lane B. F., 2003, *ApJ*, 589, 199

Delplancke F., Gorski K. M., Richichi A., 2001, *A&A*, 375, 701  
 Dominik M., Sahu K., 2000, *ApJ*, 534, 213  
 Done C., Davis S. W., Jin C., Blaes O., Ward M., 2011, *MNRAS*, 420, 1848  
 Erickcek A. L., Law N. M., 2011, *ApJ*, 729, 49  
 Goldberg D. M., Wozniak P. R., 1998, *Acta Astron.*, 48, 19  
 Han C., Kim T. W., 1999, *MNRAS*, 305, 795  
 Hog E., Novikov I. D., Polnarev A. G., 1995, *A&A*, 294, 287  
 Honma M., Kurayama T., 2002, *ApJ*, 568, 717  
 Hosokawa M., Ohnishi K., Fukushima T., 1997, *AJ*, 114, 1508  
 Inoue K. T., Chiba M., 2005, *ApJ*, 634, 77  
 Jovanović P., Zakharov A. F., Popović L. Č., Petrović T., 2008, *MNRAS*, 386, 397  
 Kayser R., Refsdal S., Stabell R., 1986, *A&A*, 166, 36  
 Keeton C. R., Moustakas L. A., 2009, *ApJ*, 699, 1720  
 Kratzer R. M., Richards G. T., Goldberg D. M., Oguri M., Kochanek C. S., Hodge J. A., Becker R. H., Inada N., 2011, *ApJ*, 728, L18  
 Krolik J. H., 1998, *Active Galactic Nuclei: From the Central Black Hole to the Galactic Environment*. Princeton Univ. Press, Princeton, NJ  
 Lee C. H., Seitz S., Riffesser A., Bender R., 2010, *MNRAS*, 407, 1597  
 Mao S., Witt H. J., 1998, *MNRAS*, 300, 1041  
 Meusinger H. et al., 2010, *A&A*, 512, A1  
 Mignard F., 2002, in Bienayme O., Turon C., eds, *EAS Publ. Ser. Vol. 2, Proc. GAIA: A European Space Project*. EDP Sciences, Les Ulis, France, p. 327  
 Miralda-Escude J., 1996, *ApJ*, 470, L113  
 Miyamoto M., Yoshii Y., 1995, *AJ*, 110, 1427  
 Novikov I. D., Thorne K. S., 1973, in DeWitt C., DeWitt B., eds, *Black Holes*. Gordon and Breach, Paris, p. 343  
 Oguri M., 2005, *MNRAS*, 361, L38  
 Paczynski B., 1998, *ApJ*, 494, L23  
 Petters A. O., Levine H., Wambsganss J., 2001, *Singular Theory and Gravitational Lensing*. Birkhäuser, Boston  
 Poindexter S., Morgan N., Kochanek C. S., 2008, *ApJ*, 673, 34  
 Pooley D., Blackburne J. A., Rappaport S., Schechter P. L., Fong W., 2006, *ApJ*, 648, 67  
 Pooley D., Rappaport S., Blackburne J. A., Schechter P. L., Wambsganss J., 2012, *ApJ*, 744, 111  
 Popović L. Č., Chartas G., 2005, *MNRAS*, 357, 135  
 Popović L. Č., Jovanović P., Stalevski M., Anton S., Andrei A. H., Kovačević J., Baes M., 2012, *A&A*, 538, A107  
 Pringle J. E., Rees M. J., 1972, *A&A*, 21, 1  
 Proft S., Demleitner M., Wambsganss J., 2011, *A&A*, 536, A50  
 Safizadeh N., Dalal N., Griest K., 1999, *ApJ*, 522, 512  
 Sazhin M. V., Zharov V. E., Volynkin A. V., Kalinina T. A., 1998, *MNRAS*, 300, 287  
 Sazhin M. V., Sazhina O. S., Pshirkov M. S., 2011, *Astron. Rep.*, 55, 954  
 Schmidt R. W., Wambsganss J., 2010, *Gen. Relativ. Gravitation*, 42, 2127  
 Schneider P., Weiss A., 1986, *A&A*, 164, 237  
 Schneider P., Weiss A., 1987, *A&A*, 171, 49  
 Schneider P., Ehlers J., Falco E. E., 1992, *Gravitational Lenses*. Springer-Verlag, Berlin  
 Shakura N. I., Sunyaev R. A., 1973, *A&A*, 24, 337  
 Sluse D., Hutsemékers D., Courbin F., Meylan G., Wambsganss J., 2012, *A&A*, 544, A62  
 Stalevski M., Jovanović P., Popović L. Č., Baes M., 2012, *MNRAS*, 425, 1576  
 Treu T., 2010, *ARA&A*, 48, 87  
 Treyer M., Wambsganss J., 2004, *A&A*, 416, 19  
 Walker M. A., 1995, *ApJ*, 453, 37  
 Williams L. L. R., Saha P., 1995, *AJ*, 110, 1471  
 Yano T., 2012, *ApJ*, 757, 189  
 Zackrisson E., Riehm T., 2007, *A&A*, 475, 453  
 Zackrisson E., Riehm T., 2010, *Adv. Astron.*, 2010, 478910  
 Zakharov A. F., 1997, *Gravitational Lenses and Microlensing*. Janus-K, Moscow  
 Zakharov A. F., Popović L. Č., Jovanović P., 2004, *A&A*, 420, 881

This paper has been typeset from a  $\text{\TeX}/\text{\LaTeX}$  file prepared by the author.